SAND78-0513
Unlimited Release

3151

25 to NTIS

A System for Detecting Neutrons in the Harsh Radiation Environment of a Relativistic Electron Beam

Lyle W. Kruse

SF 2900 Q(7-73)

Issued by Sandia Laboratories, operated for the United States Department of Energy by Sandia Corporation.

Printed in the United States of America

Available from
National Technical Information Service
U. S. Department of Commerce
5285 Port Royal Road
Springfield, VA 22161

Price: Printed Copy $4.50; Microfiche $3.00

SAND78-9514
Unlimited Release
Printed June 1978

SYSTEM FOR DETECTING NEUTRONS IN THE HARSH RADIATION ENVIRONMENT OF A RELATIVISTIC ELECTRON BEAM

Tyler W. Kruse
Beam Source Applications Division 5232
Sandia Laboratories
Albuquerque, NM 87185

ABSTRACT

Newly developed detectors and procedures allow measurement of neutron yield and energy in the harsh radiation environment of a relativistic electron beam source. A new photomultiplier tube design and special gating methods provide the basis for novel time-of-flight and total-yield detectors. The technique of activation analysis is expanded to provide a neutron energy spectrometer. There is a demonstrated potential in the use of the integrated system as a valuable diagnostic tool to study particle-beam fusion, intense ion-beam interactions, and pulsed neutron sources for simulating weapons effects. A physical lower limit of 10^8 neutrons into 4π is established for accurate and meaningful measurements in the HER environment.

ACKNOWLEDGMENTS

The author wishes to thank the personnel of Sandia Simulation Instrumentation Division 1126 for excellent oscilloscope coverage of the electron beam tests. Acknowledgment is also due to J. M. McKenzie and R. E. Jones of Sandia for their invaluable assistance in obtaining the code JUNFLD and discussing its applications. With the help of these individuals, a difficult task became manageable.

CONTENTS

ILLUSTRATIONS

A SYSTEM FOR DETECTING NEUTRONS IN THE HARSH RADIATION ENVIRONMENT OF A RELATIVISTIC ELECTRON BEAM

Introduction

Recently several laboratories have used relativistic electron beam (REB) accelerators to study controlled thermonuclear fusion,[1] to generate intense ion beams,[2] and to provide neutron sources for simulation of weapons effects.[3] Useful diagnostics for neutrons produced by REB accelerators depend on detectors which can:

- Determine the total number of neutrons from a burst
- Define the temporal behavior of the neutrons
- Accurately determine the distribution of neutron energy
- Detect neutrons with high efficiency
- Operate satisfactorily in the harsh electromagnetic and x-ray environment of the REB.

Since a single detector could not meet the requirements, three separate systems were combined to achieve the desired results:

- A neutron time-of-flight spectrometer
- Detectors that determine total neutron yield
- A neutron energy spectrometer.

Several formidable problems related to background radiation must be overcome in order to detect neutrons from an REB experiment. Sources of the most serious background radiation are:

- The intense electromagnetic pulse produced by the fast-pulse rise times and high currents of the advanced electron-beam fusion accelerators
- The large burst of bremsstrahlung which can render certain types of neutron detectors useless
- Nonthermonuclear neutrons, e.g., from photodisintegration or from interactions of ions accelerated by the diode fields.

The most direct method to measure the time history and, to some extent, energy distribution of a neutron pulse is time-of-flight. The short pulse of accelerator power (10- to 70-ns full width half maximum) and short burn (≈ 4 ns) of the thermonuclear pellet require a fast detector. A scintillation counter that combines a scintillator and a photomultiplier tube can meet the response time and detect neutrons with high efficiency.

In the high x-ray background, time-of-flight (TOF) alone cannot meet the detection requirements. Two additional detectors provide the remainder of the necessary information. A total-yield detector measures the total number of neutrons independent of energy. An activation analysis system, including a multi-material sample and a pneumatic transfer loop, is used to obtain neutron spectral information.

The complete neutron diagnostic system is shown in Figure 1. The system operates according to the following sequence:

- The activation sample is sent from the screened enclosure to the irradiation point
- The accelerator fires, automatically gating the TOF and total-yield detectors
- After the pulse, the activation sample is transferred to the counter within the screened enclosure
- Analysis begins as soon as the sample returns and continues for a predetermined count period; during that period, raw data obtained by the detectors is analyzed to provide as much information as possible on the neutron spectrum
- Analysis reveals the specific activity for each nuclide included in the sample
- Information on these specific activities, the time-of-flight (TOF) and total yield is input into an integral unfolding code which determines the number of neutrons as a function of energy.

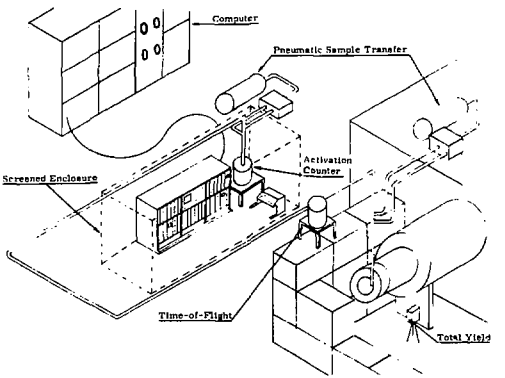

Figure 1. Neutron Diagnostic System

Neutron Time-of-Flight

The x-ray background from a typical REB is enough to overwhelm a bare photomultiplier tube. If a scintillator is added to the tube, x-rays completely saturate the tube, making measurements impossible. Shielding these detectors to prevent saturation requires such massive amounts of lead that only high-neutron yields ($> 10^{10}$) can be detected. Another problem with the use of lead shielding is the change of the neutron spectrum as shown in Figure 2. Here, a fission neutron spectrum was measured after it had passed through lead of various thicknesses.[4] Attenuation alone occurs to a thickness of 25 cm, after which the neutron spectrum changes. Therefore, the TOF detectors were designed with less than 25 cm of shielding in order to maintain high-detection efficiency and prevent spectral degradation.

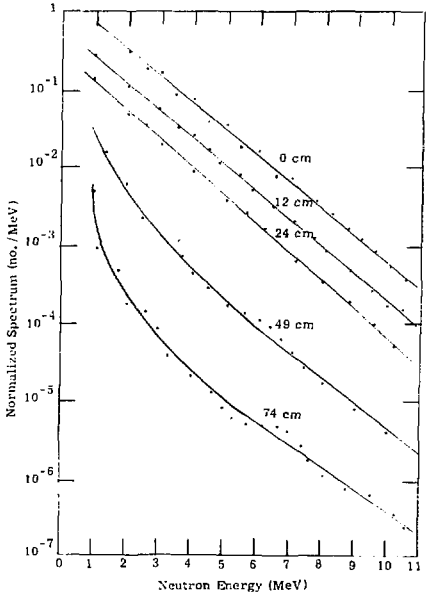

Figure 2. Fission Neutron Energy Spectra Changes Produced by Various Thicknesses of Lead

A substantial x-ray background remains even with 25 cm of lead. Since the x-ray pulse arrives before the neutrons, proper gating precludes detection of the remaining background while maintaining maximum neutron-detection efficiency. Several methods for gating photomultiplier tubes have been reported.[5,6,7] Most have deficiencies which make them unsuitable for REB applications, e.g., their turn-on times are too slow and/or the attenuation ratio between their ON and OFF states is not high enough. In some instances, nonlinear response, ringing, and spurious pulses were encountered.

In this work, three gating methods were developed which eliminated these difficulties. Although all three are useful, only the last version, which uses an RCA[8] photomultiplier tube built to the author's specifications, performed well in the most severe REB environment. Details of these gating methods are presented in Appendix A.

Figure 3 shows the basic construction of the final TOF detector. The external shield-can reduces electrical noise. The 20-cm lead used for x-ray shielding adequately excludes magnetic fields from the photomultiplier tube. Finally, a container that is 12 cm dia. by 12 cm long holds NE-224[9] liquid scintillator and is in intimate contact with the face of an RCA[8] 7265-13 photomultiplier tube.

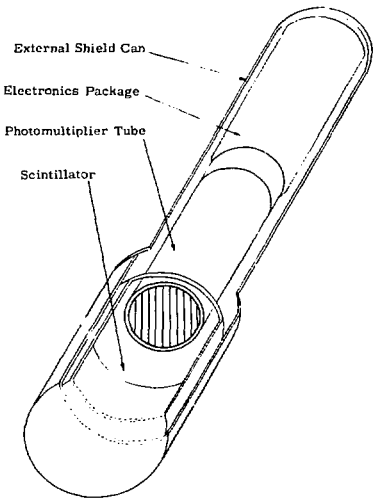

Figure 3. Basic TOF Detector Construction

A combination of focus and dynode control gates the detector. Unitrode GA-201-A silicon control rectifiers (SCRs)[10] are the active control devices in the gating circuit. Figure 4 is a schematic showing circuit wiring details of the photomultiplier base. In the OFF state, SCRs 1, 2, and 3 reverse the bias of the photocathode-focus region of the tube and SCRs 3 and 4 allow their respective dynodes to assume the potential of adjacent dynodes. In the OFF state, therefore, the SCRs exclude photoelectrons from the dynode structure, and curtail dynode multiplication. The trigger pulse shown allows the SCRs to return the controlled electrodes to their proper potentials, thereby gating the detector.

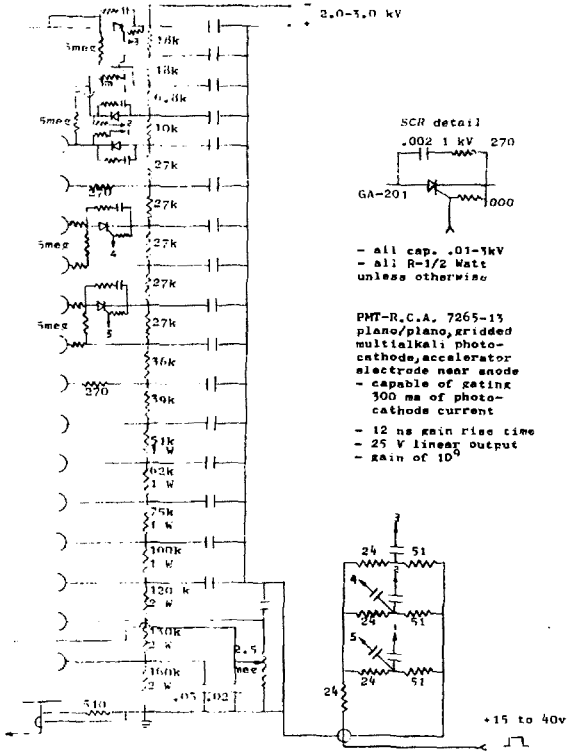

Figure 4. Wiring of Photomultiplier Base

Details of the response of the TOF detector are included in Appendix A. The detector has operated satisfactorily in the environment of the HERMES II accelerator[11] which produced 3000 R x-ray dose at one meter. Deployed at a distance of 7 m, these devices were able to detect as few as 10^7 neutrons in a single pulse. In Section II, additional experimental results are discussed.

Total Neutron Yield

In early 1966, Los Alamos Scientific Laboratories (LASL)[12] developed the silver counter which has been widely applied as a total-yield detector. Figure 5 shows a cross-sectional view of the silver-activation detector. Four Geiger Mueller (GM) tubes in parallel are individually wrapped with silver foil and imbedded in a polyethylene moderator. Incident neutrons are moderated by the polyethylene and activate the silver foil from the two capture reactions:

$$^{107}Ag(n,\beta^-)^{108}Cd$$

$$^{109}Ag(n,\beta^-)^{110}Cd$$

A scaler counts the β^- decay for one minute after a neutron burst.

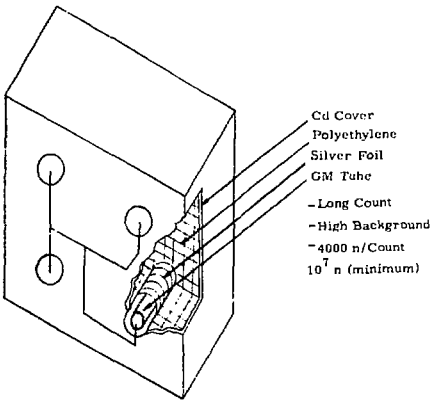

Figure 5. Cross Section of Silver Activation Detector

The basic limitation of the silver counter is that, by using GM tubes, discrimination against radiation other than β^- decay is impossible. This results in a detector that has a background on the order of 200 cpm; its inherent sensitivity of 1 count/4 x 10^4 neutrons at 12 cm requires at least 10^7 neutrons before good statistics can be obtained.

A new total-yield detector developed to eliminate these sensitivity and background problems is shown in Figure 6. Heavy water moderates incident neutrons which then undergo (n, α) reactions in the scintillator. Because the α particle produces such a large light output in the scintillator, pulse-height discrimination can readily exclude other radiations.

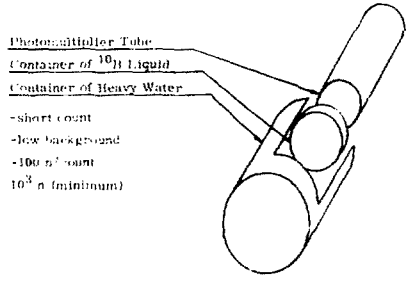

Figure 6. Total Yield Detector (^{10}B liquid scintillator)

Figure 7 shows the characteristic features of thermal neutron buildup and subsequent decay following a burst. The time delay between the initial burst and peak population is the moderation time (t_m). D_2O was selected because the low capture cross section provides the longest detector active time (t_d) of any moderator. This active time is the net diffusion time resulting from leakage and capture. The counter is gated to count for time t_d.

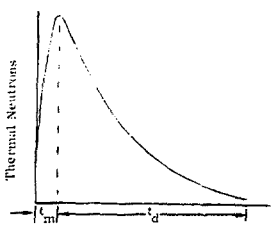

Figure 7. Detector Active Time

For the D_2O moderator, (t_m = 50 μs and t_d = 0.58) as compared to polyethylene where t_m = 20 μs and t_d = 300 μs). The detector uses a cylindrical container of D_2O moderator that is 12 cm in diameter and 12 cm long. Inside the moderator cylinder is a wafer-shaped container of NE-311A[9] that is 5 cm in diameter and 3 mm thick. The scintillator is in contact with an RCA 7265-13 photomultiplier tube. Construction of this detector is similar to that of the TOF detector pictured in Figure 3, but includes a wrapping of boron-loaded plastic between the moderator and the external shield can. This wrapping prevents scattered thermal neutrons from entering the detector.

The circuitry for the total-yield detector is similar to that shown in Figure 4 except for the SCRs and the triggering method. In this case, the SCRs are Unitrode pr-200[10] photo-SCRs. Each uses a Monsanto[13] MV10-A light-emitting diode (LED) as a combination trigger and driver. In order to operate over a period of 0.5 s, the SCRs must maintain low resistance. This is done by leaving the LED drivers on during the detector's active phase.

Because of the long delay time and because the small scintillator is insensitive to x-rays, these total-yield detectors do not have lead shielding. The background was found to be as low as one or two counts per active period. The detector has a high inherent sensitivity of 1 count/10^2 neutrons. This system requires as few as 10^4 neutrons for good statistics in comparison with the 10^7 needed for the silver counter.

Neutron Activation Analysis

The technique of activation analysis has been used for many years for neutron dosimetry and spectral analysis.[14,15] Neutron activation is accomplished by using nuclear reactions to change stable isotopes within a given sample into radioactive isotopes. The radiations emitted by the activation products are then measured and their spectra analyzed. The activation system consists of

a. A Flex-o-Rabbit pneumatic transfer[16] system for sample transfer,

b. An Ortec 6240[17] 4096-channel multichannel analyzer (MCA) and several single-channel analyzers to analyze the spectrum and measure the decay constants of the nuclides produced,

c. An interactive link to the Sandia Time-Share Computing System for handling and analyzing data.

By using a number of isotopes, each with different energy-dependent cross sections, it is possible to infer the energy spectrum of the incident neutron beam. The differential neutron spectrum can be obtained from the activated isotopes as a solution to the integral equation

$$a_i = \int_{E_1}^{E_h} \sigma_i(E)\phi(E)dE \qquad (1)$$

where

a_i is the activation of the ith isotope

σ_i is the differential cross section of the ith isotope

E_l and E_h are the energy limits of the neutron spectrum

$\phi(E)$ is the unknown neutron spectrum to be estimated.

The nuclides used in the sample were chosen according to their threshold energy, activation cross section, and the half-life of the reaction products. These criteria are in keeping with the need to acquire accurate data within a few hours of the irradiation. For a given sample, nuclides are also selected to prevent overlap of the photopeaks.

Figure 8 shows the results of a calculation of detectable neutron yield which is typical of the useful nuclides.

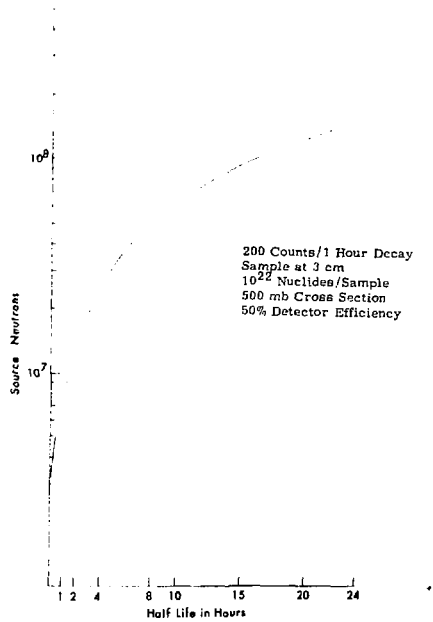

Figure 8. Detectable Neutron Yield Based on 200 Counts in a Photopeak During the First Hour of Decay

Half lives of up to as much as 20 hours, combined with the need to obtain a few hundred counts in a decay photopeak within 1 hour, limit accurate measurements to fluences greater than 10^7 neutrons cm^2.

A pneumatic transfer system (rabbit)[16] places the sample container inside a REB diode as close to the neutron source as practical. It also allows minimum-delay counting of the short half-lived (on the order of seconds) samples. After it is irradiated, the sample is transferred to a Gamma Spectroscopy System (GSS) to be measured.

To enhance the energy spectrum definition, sulfur and copper are activated independent of the rabbit system. The activated sulfur is β^- unstable and is counted in a shielded enclosure with a GM tube. The ^{62}Cu nuclide from the $^{63}Cu(n, 2n)$ reaction emits a positron which is counted by a standard gamma-gamma spectroscopy system which measures annihilation radiation.

Initially, the proof-of-principle system used NaI(Tl) detectors which were able to resolve the photopeaks of a maximum of four nuclides per rabbit sample. These samples plus the copper and sulfur provide a minimum of six sets of activation data for use in unfolding the neutron spectrum.

Specific activity measurements are insufficient by themselves to allow for an energy-spectrum solution because R_i (1) is mathematically underdetermined. However, there is additional information relative to ϕ (E) which can be used to solve the equation.

The integral unfold code IUNFLD[18] can provide a mathematically rigorous solution based on use of the total neutron yield, a trial spectrum, the first and second derivatives ($\phi'(E)$, $\phi''(E)$), and equality or inequality constraints such as $\phi(0)=0$, or $\phi(E)\geq 0$. Even an approximation to the above quantities is useful, provided their uncertainties are known. The code has the capability of weighting the data according to its uncertainty. Propagation of the weights through the IUNFLD statistical package provides the basis for assigning a confidence level to the unfolded spectrum.

Data obtained from the TOF and the total-yield systems can provide the additional information required to achieve a solution. Total-yield gives the total integral which constrains the solution. The TOF data provides inequality constraints so that $\phi'(E)$ can be estimated. Although the magnitude of $\phi'(E)$ may be uncertain, in practice knowing the direction or sign of $\phi'(E)$ aids the solution.

IUNFLD represents $\phi(E)$ as a linear sum of basis functions according to the equation

$$\phi(E) = \sum_{J=1}^{N} C_j D_j(E) \qquad (2)$$

where

$B_j(E)$: are the basis functions
C_j: are amplitude terms
N: is the number of functions

Since the distribution of the basis functions is somewhat arbitrary, proper selection can be used to advantage. The code can be started by placing more than one basis function near a structure (e.g., a spike of monoenergetic neutrons) in $\phi(E)$.

Section II. Experimental Results

Time-of-Flight and Total Yield

As a partial test of the neutron diagnostic technique, two TOF and several total-yield detectors were used to measure neutrons from the HYDRA[19] accelerator. The accelerator parameters for this experiment were a 500-keV, 110-kA, 120-ns electron beam pulse.

The experimental arrangement is shown in Figure 9. The TOF detectors were placed in the laboratory at forward angles of 42° and 32° and were gated on after the x-ray burst. Neutrons were produced via ion acceleration, using the $d(d,n)^3He$ (Q = 3.3 MeV) and $^7Li(d,n)^8Be$ (Q = 15.0 MeV) reactions. Deuterons from a deuterated polyethylene film on the anode were accelerated across the diode and, at the cathode, interacted with target materials consisting of LiCl and/or TiD_2.

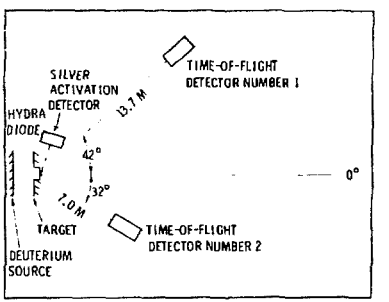

Figure 9. Schematic of the Experimental Layout Used for HYDRA Measurement. The anode-cathode separation was 1 cm.

These reaction mechanisms could be expected to occur with the failure of a fusion-target experiment. Should the target leak, fail to compress properly, or disassemble, deuterium and/or tritium would enter the diode. The ions thus released would be accelerated by the fields in the diode and would interact to produce neutrons of non-thermonuclear origin. In general these neutrons will possess large amounts of center-of-mass energy and will be distributed anisotropically. TOF deployment at different angles and distances can discriminate both of these effects.

Figure 10 shows TOF data for several possible reactions. When there is no neutron-producing material in the diode, no signal is present from either detector. The spectrum for the d-Li targ may be noted to be a composite of the spectra of the deuterium and lithium targets respectively.

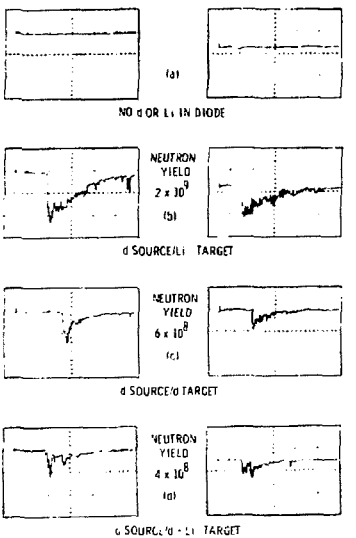

Figure 10. Scope Traces of Detector Response from Several HYDRA Experiments. The graphs on the left correspond to detector 1 and those on the right to detector 2. The sharp positive pulse at the beginning of the traces is a timing fiducial point. All sweeps are at 400 ns/div and 4.0 V/div.

Timing information obtained from shots in which both neutron groups are present is illustrated in Figure 11. The neutron arrival time at each detector is plotted against the detector's distance from the source. Instrumental delay times have been removed. Each data point is averaged from three shots and the size of each square represents the error in measurement. The arrow indicates the time at which diode current begins to rise in the accelerator.

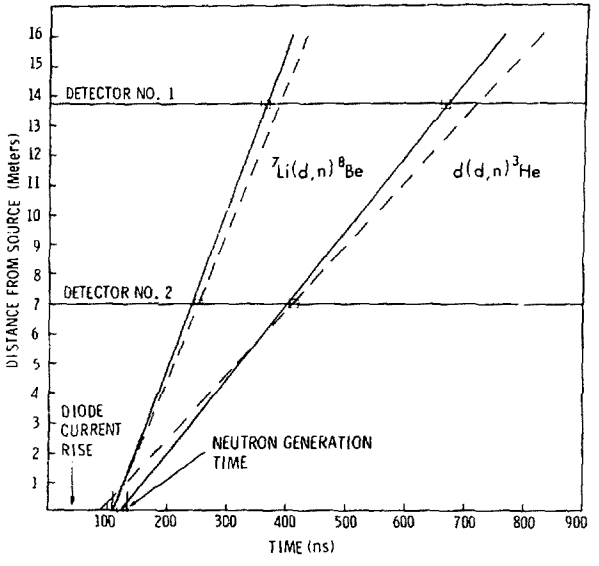

Figure 11. Arrival Time of a Neutron Group at the Detector Plotted Against the Distance of the Detector from the Source

The slopes of the solid lines in Figure 11 were calculated from the geometric position of the detectors by assuming a 500-keV incident deuteron energy and by solving the exoergic kinematics equation for the reactions. These slopes were then drawn through the data to be consistent with neutron generation time. The dashed lines were obtained by following similar procedures except that thermal energies were assumed for the deuterons.

The time of initiation of neutron generation, deduced from the solid lines, is the same for both neutron groups within the experimental accuracy. This generation time agrees well with independent Faraday-cup measurements[20] of the ion current at the cathode. The fit of the solid lines to the data (Figure 11) and the anisotropy (Figure 10) clearly indicate an incident deuteron energy of 500 keV.

The TOF detectors are deployed at different angles to the diode axis so that isotropic fusion neutrons can be distinguished from anisotropic beam-target neutrons. The distances were selected to facilitate measurement of neutron center-of-mass energy. These distances represent a required minimum yield of 10^7 neutrons for this experiment.

Full System Measurements

As a further test of the full system, an experiment was performed using the three types of detectors and a rabbit sample consisting of roughly equal amounts of Na, F, Mg, and Fe (sample details are listed in Appendix A). The HERMES II accelerator generated 10^{13} neutrons from the ^{7}Li(d, n)^{8}Be reaction. The rabbit, sulfur, and copper samples experienced a fluence of 10^8 n/cm^2.

Figure 12 shows data with the TOF detectors at 27 meters. Energies listed under T-O-F are deduced from the labeled structure of the scope traces. Maximum expected energies as calculated from the kinematics equations are also listed.

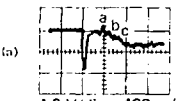

(a)

4.0 V/div 400 ns/div

^{13}C(P,N) ^{13}N

T-O-F Energy (MeV)		Kinematics Energy MeV
a	3.9	
b	3.1	2.6 max
c	2.0	

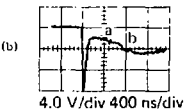

(b)

4.0 V/div 400 ns/div

^{12}C(D,N)^{13}N

Energy (MeV)		Energy MeV
a	4.19	4.7 max
b	1.29	

Production of ^{13}N*

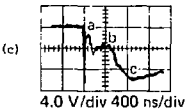

(c)

4.0 V/div 400 ns/div

^{7}Li (D,N)^{8}Be

Energy (MeV)		Energy (MeV)
a	9.34	
b	2.96	15.3 max
c	1.8	

Production of ^{8}Be*

Figure 12. Scope Traces, Time-of-Flight Neutron Energies, and Kinematic Energies for the Three Reactions Induced by the HERMES II Accelerator

These neutron energies, in Figure 12, may correspond to a number of ^{7}Li reactions. The possibilities are

(1) $^7Li(d,n)^8Be$ + 10.0 MeV

(2) $^7Li(d,n)^8Be$

excited states of ^8Be at 2.9, 6.0, and 11.4 MeV

(3) $^7Li(d,n2)^4He$ + 15.12 MeV

(4) $^7Li(d,\alpha)^5He$ + 14.1 MeV

(5) $^7Li(d,np)^7Li$ - 2.2 MeV

(6) ^{7}[illegible] MeV.

Another contribution to the neutron spectrum results from bremsstrahlung which produces photo-disintegration of deuterium. This (γ,n) yield was determined experimentally by placing deuterated polyethylene just outside the diode and adjacent to the anode. In this manner, all neutrons except those produced by the desired reaction were eliminated. For this experiment, the (γ,n) yield was 10^{10} neutrons for each of the deuterium reactions identified in Figure 12.

The result of a measurement[2] of the energy-dependent neutron yield from ^{7}Li reactions is shown in Figure 13. This spectrum was used to test the activation system. With a preliminary [illegible] sample, only the photopeak from the Na reaction was resolved. This peak plus those from the copper and sulfur samples provided a relatively good match to the reference d-Li spectrum based on observed activities.

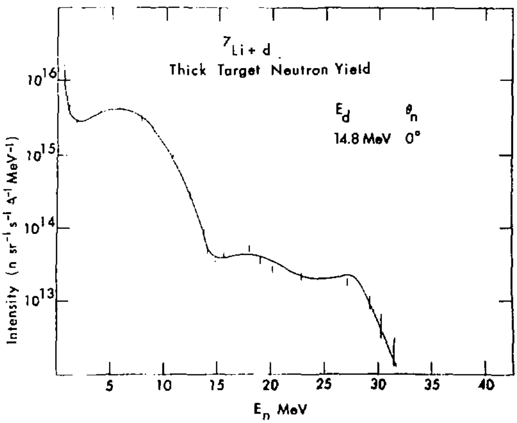

Figure 13. Neutron Yield by ^{7}Li Reactions

Activation peaks from three other groups of nuclides in the rabbit were masked by the coincidence-sum effect of the NaI(Tl) well-crystal which was used as a detector (this effect is discussed in Appendix A). As a result, insufficient information was available for IUNFLD to produce a solution. To provide the best possible spectrum solution, a higher resolution detector system is being developed.

Measurement Uncertainties

The dominant uncertainties in the measurements are related to:

- TOF neutron energy determination
- Cross section uncertainties
- Data handling procedures.

For yields on the order of 10^7 to 10^8 neutrons, the exoergic energy release cannot be measured to great accuracy. This uncertainty has been found to be approximately ±50 keV for all incident ion energies above 200 keV. As the total yield increases, accuracy is limited to an energy increment corresponding to 10 percent of the TOF oscilloscope sweep speed or to the detector-response time, whichever is greater. When a 50-ns/cm sweep is used, for example, TOF is usually limited to ±5 ns. For faster sweeps, overall accuracy is limited by the detector response time of 2 ns.

The total-yield detectors are calibrated with monoenergetic neutron sources. The scattering cross section variation of D_2O coupled with the lack of knowledge of the experimental spectrum limits total-yield accuracy to a factor of two. This factor is the tolerance which is input to IUNFLD. For the special case of monoenergetic neutrons, total yield can be measured to within ±15 percent.

The largest sources of error in the activation analysis are based on cross-section uncertainty and the behavior of the PEAKDAT code for the NaI(Tl) detector data. The cross sections for the reactions listed in Table A-2 are ±10 percent accurate. As shown in Appendix B, PEAKDAT will calculate specific activity to within ±6 percent. The sum of these is used as a best estimate tolerance of ±16 percent for IUNFLD.

The uncertainty of the IUNFLD solution is not the same as the cumulative error from the measurements. Since IUNFLD effects a minimal-norm solution to the given data within tolerances, the Chi-squared output provides a confidence level to which the solution spectrum can be believed. For the differential spectrum, values of 70 to 80 percent are good with the latter considered excellent (80% confidence is best thought of as obtaining the same spectrum, within tolerance, 80 times if the experiment were conducted 100 times). Values near or in the 90 percent range are unrealistic because uncertainties in the data do not justify such confidence in the results.[23]

Section III. Future System Improvements

To overcome difficulties experienced when measuring activation, a new detector system is being developed. Two Ortec TEC-20 Ge(Li) detectors have been multiplexed in a face-to-face geometry. Although this system has an overall efficiency of only 28 percent of that of a NaI(Tl)-well crystal, the high resolution (e.g., 2.1 keV at 1.33 MeV) allows the effective use of up to four times as many nuclides per sample. The decreased efficiency coupled with an increased peak-to-compton ratio combine to reduce the minimum detectable fluence by a factor of only two. Therefore, the lower limit of 10^{8} neutrons into 4π should be realized for the upgraded activation system.

Section IV. Conclusions

A neutron detection system capable of operating in the harsh radiation environment of a REB has been developed and tested. By employing three different types of detectors, the system can perform energy-spectrum and total-yield measurements.

If a single measurement (using only one method) were made, the inherent limitations of the detectors would make it difficult to meet the requirements outlined earlier. The difficult task of characterizing neutrons in the REB environment has been accomplished by developing a consistent set of parameters from the many complimentary measurements.

References

1. G. Yonas et al, Nucl. Fusion 14, 731 (1974).

2. P. E. Bolduc and L. W. Kruse, "Generation of 7-10 MV, 10-50 kA Pulsed Ion Beams," APS Plasma Physics Meeting, Nov.(1977).

3. P. E. Bolduc and L. W. Kruse, to be published.

4. V. N. Avaev et al, Atomnaja Energija 15, 20 (1963).

5. K. B. Keller, Rev. Sci. Instrum. 35, 1360 (1964).

6. G. Charpak, Nucl. Instrum. Meth. 51, 175 (1967).

7. D. Ben-Zeev et al, Nucl. Instrum. Meth. 114, 513 (1974).

8. RCA is a registered trademark of RCA Electronic Components, Harrison, NJ 07029.

9. Available from Nuclear Enterprises Inc., 935 Terminal Way, San Carlos, CA 94070.

10. Unitrode is a registered trademark of Unitrode Corp., Watertown, MA 02172.

11. T. H. Martin, K. R. Prestwich, and D. L. Johnson, "Summary of the Hermes Flash X-Ray Program," SC-RR-69-421, Sandia Laboratories, Oct.(1969).

12. R. J. Lanter and D. E. Bannerman, Los Alamos Scientific Laboratory report LA-3498-MS, July 1966.

13. Monsanto Corp., 10131 Bubb Road, Cupertino, CA 95014.

14. Nargol Walla and Przybylowicz, Activation Analysis with Neutron Generators, John Wiley & Sons (1973).

15. P. Kruger, Principles of Activation Analysis, John Wiley & Sons (1971).

16. Reactor Experiments Inc., 963 Terminal Way, San Carlos, CA 94070.

17. Ortec Inc., 100 Midland Road, Oak Ridge, TN 37830.

18. F. Biggs and D. Amos, IUNFLD, "Numerical Solution of Integral Equations and Curve, Figging," SC-RR-71-0212 and SAND77-0136, September 1971, and R. E. Jones, J. M. McKenzie, and L. A. Romero, "Differential Neutron Spectra Unfolding from Foil Activation Data," IEEE, Proc. Nuc. Sci., Dec. 1977.

19. J. J. Ramirez and L. W. Kruse, Rev. Sci. Inst., 47, 832 (1976).

20. D. W. Swain, L. P. Mix, L. W. Kruse, and J. W. Poukey, "Measurements of Large Ion Currents in a Pinched REB Diode," Journal of Applied Physics, pp. 48, 118 (1977).

21. M. A. Lone et al, Nucl. Inst. and Meth. 143, 331 (1977).

22. R. L. Heath, "Scintillation Spectrometry Gamma-Ray Spectrum Catalog," IDO-16880, Vol. 1 (1964).

23. R. E. Jones, private communication (March 1978).

APPENDIX A

Details of Detector Development

Time-of-Flight (TOF)

The earliest version of TOF detectors used a 12.7-cm-diam x 12.7-cm long plastic scintillator coupled to a 12.7-cm-diam photomultiplier tube (RCA 4522). This detector proved worthless when exposed to the Hermes II environment.

Two problems became apparent after several failures. First, x-ray backgrounds, despite 45 cm of lead shielding, was intense enough to cause the high-resistivity S-11 photocathode of the 4522 to sag in potential. This sag takes time to correct and focus before the tube can be used again. Full recovery is impossible in the few hundred nanoseconds of neutron observation. Furthermore, 45 cm of lead shielding is not acceptable.

To overcome this problem, a new photomultiplier tube was fabricated to my specifications by RCA. This tube (7265-13) uses a 14-stage multiplier structure that incorporates an accelerator grid between the last two dynodes. The grid maintains proper electron focus which allows a high-linear-output current by using a tapered-chain divider.

The photocathode is multialkali (Na-K-Cs-Sb) with lower resistivity than an S-11 cathode. In addition, an internal metallic grid is deposited over the photocathode so that if local sag occurs, proper focus is maintained.

A plano-plano front end reduces the high capacitance which is normally present in a spherical-section input such as the 4522. This feature greatly reduces switching times when controlling the focus region of a photomultiplier tube.

At room temperature, a normal S-11 photocathode will sag in potential with 10^{-8}A of steady photocathode current. It was found to sag at 63-μA 120-ns pulsed current from HERMES II.

The work function of the modified photocathode is approximately 1.1 eV. Since scintillator photons are predominately 2.7 eV, 1.6 eV photoelectrons are generated at the photocathode. In the OFF state (Figure A1), dynode 1 and the focus plane are tied together to prevent a potential well. These electrodes are then tied to +52.4 V. The photocathode is tied to +104.8 V resulting in the reverse field shown in Figure A1.

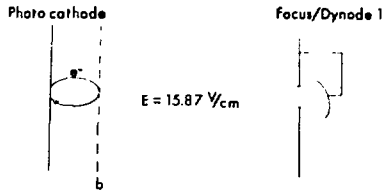

Figure A1. Reverse Biased Focus Region

The potential in space at point b (1 mm from the photocathode) is 1.6 eV; the electron trajectory shown can be calculated as:

$$\text{initial velocity: } 1/2\ mV^2 = KE \Rightarrow V = \frac{2(1.6\times10^{-19})(1.6\ eV)}{9.11\times10^{-31}\ kg} \tag{A1}$$

$$V = 7.49 \times 10^5\ m/s$$

At point b the electron velocity is zero so the field acceleration can be calculated

$$0 = V = (7.49 \times 10^5)^2 + 2(-a)(1\times10^{-3}) \Rightarrow a = -2.81\times10^{14}\ m/s \tag{A2}$$

Time from electron emission to subsequent collection at the photocathode in the OFF state is then:

$$(-2.81\times10^{14})t^2 + (8.38\times10^5)t = 0 \tag{A3}$$

$$t = \frac{8.38\times10^5}{2.81\times10^{14}} = 2.98\ ns$$

This single electron treatment is valid only to the limit of the space charge which can be sustained under these conditions. The space charge-limited current can easily be calculated for the plano-plano front end as:

$$ib = \frac{2.336\times10^6 eb^{3/2}}{d^2}\ (amp/cm^2)$$

$$ib = \frac{2.336\times10^6\ (15.87)^{3/2}\ 17.35\ cm^2}{(3.3)^2} \tag{A4}$$

$$ib = 235\times10^{-6}\ A\ .$$

This value of current is four times the pulsed sag current observed and, in fact, the tube has successfully gated a $.40 \times 10^{-3}$ A 250-ns photocathode current pulse without a sag.

The second problem encountered was choosing a scintillator. The x-ray background was sufficiently intense to create high levels of excitation of a 100-ns component in the plastic scintillators. Although secondary components are present in all scintillators, they are normally of such low intensity that they do not interfere with the primary component. However, there was enough light in the 100-ns component to overwhelm the photomultiplier tube when it was gated on after the x-ray burst. Previous experience with light pipes made of plastic indicates that the efficiency of this component may be related to a lattice that allows transfer of this flourescence. A similar 100-ns component is not directly excited in nonscintillator plastic.

By changing to the 224 liquid scintillator, the 100-ns component was reduced by a factor of 150. Response of the detector, using the new tube and scintillator in the HERMES II environment, is shown in Figure A2.

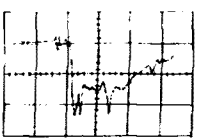

4×10^{8} total neutrons d-d and $d-^{7}$Li

1.6 V/div 100 ns/div

Figure A2. Detector Response in HERMES II Environment

It was finally determined that when gating is done only by controlling the dynodes, as with earlier detector versions, it is not enough to prevent saturation of the photomultiplier tube. Adding the reverse-bias front end resulted in such insensitivity to saturation that the TOF detector finally chosen has not become saturated even with a total dose of 2000 Rad in 120 ns. Fast switching times and linear response have not suffered; detector rise time from OFF to ON state is 16 ns, the signal rise time 2 ns, and linear output 1.2 A into 50 ohms.

Activation Analysis

As previously mentioned, samples to be activated are constructed by loading a Rabbit capsule with a homogeneous mechanical mix of powder containing the isotopes. Table A1 shows two samples suitable for NaI(Tl).

TABLE A1

Activation Samples

	Nuclide	Number Density (atoms/cm^3)
Sample 1	Ni	4.76×10^{21}
	Si	7.55×10^{21}
	Mg	9.52×10^{21}
	O	2.84×10^{22}
Sample 2	Na	1.55×10^{22}
	F	1.55×10^{22}
	Mg	1.19×10^{22}
	Fe	1.75×10^{22}

The compounds, such as SiO_2, MgO, and NaF, are powders so that the final number densities are slightly lower than normal solid densities.

The detector chosen for the early tests was a 3" NaI(Tl) well crystal, but the coincidence-sum of the principle radiations from the high-speed sample masked all but the lowest energies, such as the 439-keV photopeak from the $^{23}Na(n, p)^{23}Ne$ reaction. Although this effect is discussed by Heath,[22] its severity is best illustrated in Figure A3.

Figure A3 illustrates two separate spectrum results from a standard 0.1 uCi ^{22}Na source. The source has the same physical dimensions as the Rabbit capsule and was placed inside the well to obtain A3(a). The same source, on the face of the detector, yielded A3(b). Nothing in published literature indicated that the full energy summation could be as severe as discovered. Therefore, despite low cost, this type of detector is clearly not acceptable for multinuclide analysis.

Multiplexing two GeLi detectors in a face-to-face geometry maintains good efficiency while eliminating coincidence-sum effects. Although total price is higher, it is probably the only reasonable choice.

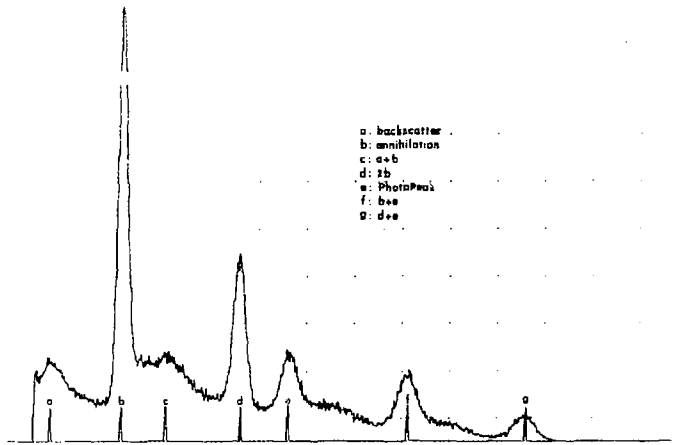

A3(a)

A3(b)

Figure A3. NaI(T1) Coincidence-sum Effect

As a final aspect, the pneumatic transfer system allows activation products with a short half-life to be measured. The cross-section library in my version of the IUNFLD code has been expanded to the 22 reactions in Table A2. While not a complete list of usable reactions, it represents the types of applicable reactions. In addition to the nuclide selection criterion previously discussed, uncertainty of cross-section values is the single largest source of errors in activation analysis. For this reason, not all nuclides which survived prior tests are suitable for use. It is not uncommon in some cases to find cross-section values which are uncertain by as much as 50 percent or more. Therefore, except in extreme cases, it is best to avoid these nuclides.

TABLE A2

IUNFLD Foil No.		Configuration	Reaction
^{239}Pu	1	B^{10} + Cd cover	(n, f)
^{238}U	2	B^{10} + Cd cover	(n, f)
^{93}Np	3	B^{10} + Cd cover	(n, f)
^{32}S	4	Bare	(n, p)
^{235}U	5	B^{10} + Cd cover	(n, f)
^{58}Ni	6	Bare	(n, p)
^{56}Fe	7	Bare	(n, p)
^{24}Mg	8	Bare	(n, p)
^{23}Na	9	Cd cover	(n, γ)
^{27}Al	10	Bare	(n, α)
^{54}Fe	11	Bare	(n, p)
^{115}In	12	Bare	(n, γ)
^{232}Th	13	Cd cover	(n, f)
^{127}I	14	Bare	(n, γ)
^{28}Si	15	Bare	(n, p)
^{16}O	16	Bare	(n, p)
^{23}Na	17	Bare	(n, p)
^{23}Na	18	Bare	(n, α)
^{19}F	19	Bare	(n, p)
^{19}F	20	Bare	(n, α)
^{65}Cu	21	Bare	(n, 2n)
^{63}Cu	22	Bare	(n, 2n)

APPENDIX B

Discussion of Computer Codes

Program PEAKDAT Printout

```
00600 PROGRAM PEAKDAT(INPUT,OUTPUT,TAPE20,TAPE30)
00610 DIMENSION BAD(10)
00620 DIMENSION Y(1024),Y1(1024),X(1024),Y2(1024),P(90),SUM(90),PT(90)
00630 CAL=3.046
00640 PRINT *,"                                    -----PROGRAM        START-----"
00650 PRINT *,"NA-I GAMMA SPECTRUM ANALYSIS"
00660 PRINT *,"DATA FILE ONEGAM RETRIEVED FOR PROGRAM"
00670 PRINT *,"111 CAL= "CAL," K.E.V./CHANNEL"
00680 CALL GETF(IERR1,20,6HONEGAM)
00690 PRINT *,"IERR1=",IERR1
00700 TCOR=2.5
00710 ASUM=0.
00720 SER=7.
00730 PRINT *,"126 SER= "SER," =1ST DERIVATIVE SEARCH LEVEL"
00740 R=5.
00750 PRINT *,"128 R= "R," CHANNELS +/- AROUND PEAK"
00760 R=R*CAL
00770 READ(20,23)(Y(I),I=1,1024)
00780 23 FORMAT(4X,10F7.0)
00790 PRINT *,"120 TCOR= "TCOR," SECONDS FOR SAMPLE TRANSFER"
00800 SAM=2.
00810 PRINT *,"142 SAM = "SAM," = STANDARD SAMPLE NUMBER"
00820 TO=(INT((Y(1)/60.)*100.+.5))/100.
00830 T=Y(1)*(-1.)
00840 PRINT *,"LIVE TIME = "T," MINUTES"
00850 WRITE(30,*)"          SMOOTHED  FIRST  DERIVATIVE  OF  RAW  DATA "
00860 I=2
00870 152 ASUM=ASUM+Y(I)
00880 X(I)=I
00890 I=I+1
00900 IF(I-1024)152,160,160
00910 160 I=2
00920 161 I=I+1
00930 Y(I)=(Y(I-2)+Y(I-1)+Y(I)+Y(I+1)+Y(I+2))/5.
00940 IF (I-1022) 161,164,164
00950 164 I=0
00960 165 I=I+1
00970 J=0
00980 Y(I)=(Y(I+1)+Y(I)+Y(I-1))/3.
00990 Y1(I)=(Y(I+1)-Y(I))/1.
01000 IF(I-1024)165,181,181
01010 181 CALL GETF(IERR1,20,6HONEGAM)
01020 PRINT *,""
01030 READ(20,23)(Y(I),I=1,1024)
01040 190 CONTINUE
01050 I=60
01060 192 IF(I-1024)194,340,340
01070 194 IF(Y1(I)-SER)200,220,220
01080 200 I=I+1
01090 GO TO 192
01100 220 IF(Y1(I)-0.)250,250,230
01110 230 I=I+1
01120 GO TO 220
01130 250 J=J+1
01140 P(J)=I
01150 PRINT *," "
01160 PRINT *,"LOCATION OF PEAK IS CHANNEL ",P(J)
01170 W=P(J)*CAL
01180 G=ALOG10(W)
01190 H=6**2.
```

```
01200 Q=.77684-.39997*G+.05453*H
01210 S=Q*W
01220 S=W-(S/2.)
01230 I=INT(S/CAL)
01240 W=INT(W)
01250 PRINT #,"DETECTOR RESOLUTION FOR "+W+" K.E.V. "
01260 Q=(INT(Q*10000+.5))/100.
01270 PRINT #,"IS "+Q+" PERCENT"
01280 300 J=J+1
01290 P(J)=I
01300 PPINT #," "
01310 I=P(J-1)+5
01320 GO TO 192
01330 340 K=J
01340 IF (K-0) 342,342,358
01350 342 PRINT #,"ZERO PEAKS HAVE BEEN IDENTIFIED"
01360 343 SER=SER/2.
01370 IF (SER.LT.2.) GO TO 570
01380 PRINT #," "
01390 PRINT #,"NEW SEARCH LEVEL IS "+SER
01400 I=60
01410 348 IF (I-1024) 349,349,343
01420 349 IF (Y1(I).GT.SER) GO TO 352
01430 I=I+1
01440 GO TO 348
01450 352 IF (I-1024) 353,350,343
01460 353 IF (Y1(I).LT.0.) GO TO 356
01470 I=I+1
01480 GO TO 352
01490 356 PRINT #,"POSSIBLE PEAK AT "+I*CAL+" K.E.V."
01500 GO TO 348
01510 358 J=1
01520 360 IDELT=P(J)-P(J+1)
01530 IMIN=P(J+1)
01540 ITOP=P(J)+IDELT
01550 Y2(J)=IDELT/2.354
01560 PT(J)=IMIN
01570 PT(J+2)=ITOP
01580 PT(J+1)=ITOP
01590 Q=(Y(ITOP)+Y(IMIN))/2.
01600 R=Y(P(J))-Q
01610 USUM=0.
01620 Y2(1024-J)=0.
01630 I=IMIN
01640 420 USUM=USUM+Y(I)-Q-R
01650 B=((2.*IDELT)**2.)/2.772589
01660 C=Y(P(J))-Q+2.
01670 Y2(1024-J)=Y2(1024-J)+C*EXP(-((I-P(J))**2.)/B)
01680 I=I+1
01690 CONTINUE
01700 IF(I-ITOP)420,460,460
01710 460 SUM(J)=USUM
01720 SUM(J)=INT(SUM(J)/.76096)
01730 CONTINUE
01740 Y2(1024-J)=Y2(1024-J)/.76096
01750 W=INT(P(J)*CAL)
01760 IF(SUM(J)-Y2(1024-J))470,478,474
01770 470 Z=(Y2(1024-J)-SUM(J))/Y2(1024-J)
01780 Z=(INT(Z*10000+.5))/100.
01790 PRINT #,W," K.E.V. PEAK IS "+Z+" PERCENT SMALLER THAN TRUE GAUSSIAN"
01800 GO TO 479
01810 474 Z=(SUM(J)-Y2(1024-J))/Y2(1024-J)
01820 Z=(INT(Z*10000+.5))/100.
01830 PRINT #,W," K.E.V. PEAK IS "+Z+" PERCENT LARGER THAN TRUE GAUSSIAN"
01840 GO TO 479
01850 478 PRINT #,W," K.E.V. PEAK IS PERFECT FIT TO TRUE GAUSSIAN"
01860 479 J=J+2
01870 IF(J-(K-1))360,360,490
01880 490 L=K/2
01890 I=0
01900 492 I=I+1
01910 X(I)=INT(X(I)*CAL)
01920 IF(I-1024)492,500,500
01930 500 PRINT #," "
01940 PRINT #," "
```

```
01950 PRINT *,"      -----PEAK ENERGY AND INTEGRATED COUNTS ABOVE BKG-----"
01960 PRINT *," "
01970 PRINT *," "
01980 PRINT *,"          ",L," PEAKS HAVE BEEN IDENTIFIED"
01990 PRINT *," "
02000 PRINT *," "
02010 PRINT *," "
02020 M=0
02030 L=1
02040 DO 550 I=1,L PRINT *," "
02050 PRINT *," "
02060 PRINT *,"            PEAK ENERGY K.E.V.          COUNTS IN PHOTOPEAK"
02070 PRINT *," "
02080 550 PRINT *,"                    ",X(P(J)),"                    ",SUM(J)
02090 FOR=-1.63349*ALOG10(X(P(J)))+5.0691
02100 FOR=INT(2.*(SUM(J)/10.**FOR))
02110 PRINT *,"     ",FOR," GAMMA RAYS EMITTED AT ",X(P(J))," K.E.V."
02120 IF (PT(J+1)-PT(J+2))561,561,555
02130 555 Z=ABS(PT(J+1)-PT(J+2))
02140 PRINT *,"THE ",X(P(J))," K.E.V. PEAK OVERLAPS THE"
02150 PRINT *,X(P(J+2))," K.E.V. PEAK BY ",Z," CHANNELS"
02160 BAD(J)=X(P(J))
02170 BAD(J+1)=X(P(J+2))
02180 M=M+1
02190 561 GO TO 715
02200 563 J=J+2
02210 IF(J-(K-1))537,537,566
02220 566 IF(M-0)570,570,680
02230 570 WRITE(30,23)(Y(I),I=1,1024)
02240 ENDFILE 30
02250 CALL REPLACE(IERR2,30,6HTWOGAM)
02260 PRINT *," "
02270 PRINT *," "
02280 PRINT *," "
02290 PRINT *," "
02300 PRINT *,"IERR2=",IERR2
02310 CALL RETURNF(20)
02320 CALL RETURNF(30)
02330 PRINT *,"CALCULATION COMPLETE"
02340 GO TO 685
02350 680 PRINT *," "
02360 PRINT *,"          -----OVERLAPPING PEAKS REFIT-----"
02370 715 IF(AM.EQ.1.) GO TO 718
02380 716 IF(AM.EQ.2.) GO TO 740
02390 717 IF(AM.EQ.3.) GO TO 563
02400 718 IF(ABS(X(P(J))-810.)-R) 725,725,719
02410 719 IF(ABS(X(P(J))-1369.)-R)730,730,720
02420 720 IF(ABS(X(P(J))-1780.)-R) 735,735,721
02430 721 IF(ABS(X(P(J))-2754.)-R)730,730,722
02440 722 PRINT *,"THIS PEAK NOT ASSOCIATED WITH SAMPLE NO. 1"
02450 GO TO 563
02460 725 EN=FOR/(1.-EXP(T*1.12313E-07))
02470 EN=EN/1.642358E+21
02480 PRINT *,"SP.ACT. FOR IUNFLD FOIL NO. 6 = ",EN
02490 GO TO 563
02500 730 EN=FOR/(1.-EXP(T*1.28361E-05))
02510 EN=EN/3.30236E+21
02520 PRINT *,"SP.ACT. FOR IUNFLD FOIL NO. 8 = ",EN
02530 GO TO 563
02540 735 EN=FOR/(1.-EXP(T*5.02281E-03))
02550 EN=EN/2.604828E+21
02560 PRINT *,"SP.ACT. FOR IUNFLD FOIL NO. 15 = ",EN
02570 GO TO 563
02580 740 IF(ABS(X(P(J))-197.)-R) 750,750,741
02590 741 IF(ABS(X(P(J))-439.)-R) 755,755,742
02600 742 IF(ABS(X(P(J))-847.)-R) 760,760,743
02610 743 IF(ABS(X(P(J))-1370.)-R) 765,765,744
02620 744 IF(ABS(X(P(J))-1630.)-R) 770,770,745
02630 745 IF(ABS(X(P(J))-1811.)-R) 775,775,746
02640 746 IF(ABS(X(P(J))-2754.)-R) 780,780,747
02650 747 PRINT *,"THIS PEAK NOT ASSOCIATED WITH SAMPLE NO. 2"
02660 GO TO 563
02670 750 EN=FOR/(1.-EXP(T*2.57676E-02))
02680 EN=EN/EXP(-TCOR*2.57676E-02)
02690 EN=EN/2.145725E+22
02700 PRINT *,"SP.ACT. FOR IUNFLD FOIL NO. 19 = ",EN
```

```
02710 GO TO 563
02720 755 EM=PQR/(1.-EXP(T*1.8241E-02))
02730 EM=EM/EXP(-TCOR*1.8241E-02)
02740 EM=EM/2.212068E+22
02750 PRINT *,"SP.ACT. FOR IUNFLD FOIL NO. 17 = ";EM;
02760 GO TO 563
02770 760 EM=PQR/(1.-EXP(T*7.46283E-05))
02780 EM=EM/2.502491E+22
02790 PRINT *,"SP.ACT. FOR IUNFLD FOIL NO. 7 = ";EM;
02800 GO TO 563
02810 765 PRINT *,"THIS PEAK IS DECAY COMBINATION OF FOILS 8 AND 17"
02820 GO TO 563
02830 770 EM=PQR/(1.-EXP(T*6.08024E-02))
02840 EM=EM/EXP(-TCOR*6.08024E-02)
02850 EM=EM/2.212068E+22
02860 PRINT *,"SP.ACT. FOR IUNFLD FOIL NO. 18 = ";EM;
02870 GO TO 563
02880 775 EM=PQR/(1.-EXP(T*7.46283E-05))
02890 EM=EM/2.502491E+22
02900 EM=EM/.29
02910 PRINT *,"SP.ACT. FOR IUNFLD FOIL NO. 7 = ";EM;
02920 GO TO 563
02930 780 EM=PQR/(1.-EXP(T*1.28361E-05))
02940 EM=EM/1.710504E+22
02950 PRINT *,"SP.ACT. FOR IUNFLD FOIL NO. 8 = ";EM;
02960 GO TO 563
02970 785 CONTINUE
02980 END
READY.



BYE

 14.24.46  78/03/10.
OFF LINE PUSE
TTY 050       1.000 CPU
```

The code PEAKDAT is a photopeak analysis routine for NaI. The code is useful only if a thorough characterization is made of the detector used. It is convenient to break the detector response into three quantities which can easily be determined experimentally: resolution (FWHM photopeak as a function of energy), Peak-to-total-ratio (ratio counts in photopeak to total counts), and detector efficiency.

Since the majority of the γ-rays observed are less than 3 MeV, the MCA is limited to 3 MeV maximum energy. This greatly simplifies detector characterization. Five calibrated standard γ-ray sources were used to determine detector response. The sources and γ-ray energies are listed in Table B1.

TABLE B1

Sources and γ-ray Energies

Source	γ-Ray Energy
^{137}Cs	661.2 KeV
^{54}Mn	835.0 KeV
^{65}Zn	1.114 MeV
^{22}Na	511 KeV
^{22}Na	1.274 MeV
^{60}Co	1.17 MeV
^{60}Co	1.33 MeV
^{60}Co	2.50 MeV

γ-ray spectrum from each of the isotopes are measured. The system is calibrated to 3.0 keV/channel, using a ^{60}Co source and an Ortec 419 precision pulse generator. From the raw data, the location of each photopeak and count in that channel are recorded. The channel locations at half the peak count are then recorded. Where these points are between channels, linear interpolation is used to determine fractional parts of a channel. The full-width-half-maximum for each photopeak is then found by multiplying the difference in channel numbers by the calibration of 3 keV/channel.

A plot of this detector resolution data appears as a concave upward curve on semilog paper. γ-ray energy on a log scale vs resolution expressed as a percent is found by dividing FWHM value by full photopeak energy. A convenient function for detector resolution can therefore be generated by a nonlinear, least-squares fit of the data to the form of Equation (B1).

$$R = a_0 + a_1, \text{ Log}(E) + a_2(\text{Log } E)^2 \qquad \text{(B1)}$$

The Normal Equations for solution are:

$$B_1 = Na_o + B_2a_1 + B_3a_2$$

$$B_6 = B_2a_o + B_3a_1 + B_4a_2$$

$$B_7 = B_3a_1 + B_4a_1 + B_5a_2$$

where:

N = number of measured values

$B_1 = \Sigma R$ = sum of resolution values R

$B_2 = \Sigma \text{Log}_{10}(E)$ = sum of log of photopeak energies

$B_3 = \Sigma (\text{Log}_{10}E)^2$

$B_4 = \Sigma (\text{Log}_{10}E)^3$

$B_5 = \Sigma (\text{Log}_{10}E)^4$

$B_6 = \Sigma \text{Log}_{10}(E) \times R$

$B_7 = \Sigma (\text{Log}_{10}(E) \times R)^2$

The Normal Equations are solved for the coefficients in Equation (B1). Detector resolution is then calculated by the routine between lines 1170 and 1270 in the PEAKDAT code.

By calculating the peak-to-total-ratio of the ^{137}Cs spectrum and knowing the calibrated activity of the source, I found the detector efficiency to be 51 percent. I assumed this efficiency would remain constant with energy. This, of course, is not the case but the difference can be accounted for in the peak-to-total function.

Using the total counts in a photopeak, the assumed efficiency value and the known source activities, peak-to-total ratios are calculated for each peak. Again, Equation (B1) is solved for the functional form of the peak-to-total ratio vs energy.

The code PEAKDAT operates as follows:

a. The raw counts/channel MCA data is written into a file.
b. The file is loaded into an array and smoothed.
c. A first derivative is taken of the smoothed data.
d. The code then begins looking for a first derivative value above some search level (SER)

c. When this condition is met, the first zero crossing of the first derivative is found (the location of a peak).

f. The code then continues until all the data has been examined. The search level can be changed and is useful in discrimination against noise.

After the peak locations are found, the resolution and channel locations at FWHM are calculated for each peak. The photopeak area is found by summation of raw data counts above the FWHM level only. The area of a rectangle of half photopeak height and FWHM width is then added to the sum. If it is assumed that the photopeak is Gaussian, the total area can then be calculated by dividing the summation by a factor of .7609%. The code then generates a true Gaussian based on photopeak height and is determined from the resolution calculation and compares the two areas. For true photopeaks, the deviation from a true Gaussian is always less than 4%. For noise-produced or coincidence-sum peaks, this deviation is generally greater than 40%.

The efficiency and peak-to-total ratio are then used to determine the total number of γ-rays emitted from the sample for a given photopeak. The code compares photopeak energies to those of expected γ-rays from the sample and calculates specific activity. Any decay during the sample transfer time is corrected.

The activities returned by PEAKDAT for the eight calibration-source energies were all within 6% of the expected values.

Several years ago, F. Biggs and D. Amos of Sandia developed program UNFOLD to solve integral equations of the first kind. R. E. Jones of Sandia has adapted this method to an interactive program IUNFLD. The big advantage of these programs is that they allow the input of auxiliary information and do not specifically need a trial spectrum. The code is mathematically rigorous and has the advantage of being interactive.

As mentioned in Section I, IUNFLD represents $\phi(E)$ as a linear sum of basis functions. The basis functions are actually B splines:

$$C_i = \sum_{j=1}^{N} C_j \int_{E_\ell}^{E_h} D_j(E)\sigma_i(E)dE = \sum_{j=1}^{N} C_j A_{ij} \quad ,$$

which results in a system of linear equations. The integral has a fixed value (A_{ij}) for each $D_j(E)\sigma(E)$. In matrix form a least-square solution of the vector C is required when AC = G.

Activation data is weighted according to its accuracy by dividing each row of the A matrix and G vector by the estimated error in G. A smaller error in the activation data therefore results

in a larger weight. These estimated errors are propagated and used in statistical tests; the solution accuracy statistics are available as part of the output package.

In order to fit the code into allotted file space of the time-share system and to provide the interactive capability, the code is broken into several files. A procedure file IUNPR2 attaches the compiled binary UNFOLD file IUNLG2 and R file.

IUNPR2

```
IF<FILE<R.,NOT.LD>>GET,R.
REWIND,P,RBIN.
FTN,I=R,B=RBIN.
ATTACH,IUNLG2/UN=REJONES.
ATTACH,CSLIB/UN=LIBRARY.
LIBRARY,CSLIB.
LOAD,IUNLG2.
LOAD,RBIN.
EXECUTE.
UNLOAD,IUNLG2,RBIN.
COMMENT.  IUNFLD EXECUTION COMPLETED.   GOODBYE.
READY.
```

The R file is designated by the user to begin code execution:

-IUNPR2(R=SPLOOK)

This file retrieves the activation cross-sections library, contains the format to read the file, and calls the FINTRP interpolation routine to generate cross sections at energies between those in the library.

SPLOOK

```
      FUNCTION R(T,I)
      DIMENSION XSAVE(70,22),YSAVE(70,22),N(22)
      COMMON/INPUT/X(60)
      DATA INIT/0/
      IF (INIT.EQ.1) GO TO 10
      INIT=1
      CALL GETF(IERR,21,5HSPCTR)
      IF (IERR.NE.0) STOP 21
      REWIND 21
        DO 5 K=1,22
        J2=0
1       J1=J2+1
        J2=J1+2
        READ(21,20) (XSAVE(J,K),YSAVE(J,K),J=J1,J2)
        DO 2 J=J1,J2
2       IF(XSAVE(J,K).EQ.0) GO TO 3
        GO TO 1
3       N(K)=J-1
5       CONTINUE
      CALL RETURNF(21)
10      M=INT(X(I))
        R=FINTRP(T,XSAVE(1,M),YSAVE(1,M),N(M),0)
      IF (R.LT.0.) R = 0.
20      FORMAT(F10.4,5F12.4)
        RETURN
        END
READY.
```

The value 22 in my SPLOOK.R file are the dimension values indicating the numbers of cross sections included in the extended library shown in Table A2.

Additional cross sections can easily be added to the SPCTR cross-section library by changing the R file dimension statements and adding the desired cross sections. (Where the first entry is energy in MeV, the cross section follows in barns.) An example of a SPCTR printout follows:

SPCTR

1.6000E-09	0.0000	5.0000E-08	0.0000	1.0000E-05	5.2373E-08
2.5500E-02	1.1409E+00	5.0000E-02	1.1744E+00	1.0000E-01	1.2406E+00
1.9000E-01	1.3832E+00	3.0000E-01	1.4010E+00	5.7500E-01	1.5136E+00
1.0000E+00	1.7257E+00	1.6000E+00	1.7954E+00	1.9000E+00	1.3694E+00
2.0000E+00	1.8962E+00	2.1000E+00	1.8960E+00	2.2000E+00	1.8982E+00
2.3000E+00	1.9801E+00	2.4000E+00	1.8603E+00	2.8000E+00	1.7841E+00
3.7000E+00	1.6947E+00	4.9000E+00	1.5775E+00	5.8000E+00	1.5644E+00
5.9000E+00	1.5609E+00	6.0000E+00	1.5593E+00	6.1000E+00	1.5872E+00
6.2000E+00	1.6246E+00	7.3000E+00	2.0357E+00	8.2000E+00	2.2287E+00
8.5000E+00	2.2288E+00	8.6000E+00	2.2289E+00	8.7000E+00	2.2290E+00
8.8000E+00	2.2290E+00	8.9000E+00	2.2290E+00	9.0000E+00	2.2275E+00
9.1000E+00	2.2166E+00	9.4000E+00	2.1791E+00	1.0000E+01	2.1129E+00
1.0100E+01	2.1177E+00	1.0200E+01	2.1225E+00	1.0300E+01	2.1273E+00
1.0400E+01	2.1322E+00	1.0500E+01	2.1370E+00	1.0600E+01	2.1418E+00
1.0700E+01	2.1466E+00	1.0900E+01	2.1563E+00	1.1500E+01	2.2116E+00
1.2100E+01	2.2732E+00	1.2700E+01	2.3464E+00	1.3900E+01	2.5438E+00
1.4800E+01	2.6062E+00	1.4900E+01	2.6085E+00	1.5000E+01	2.6089E+00
1.5100E+01	2.6074E+00	1.5200E+01	2.6038E+00	1.5300E+01	2.5869E+00
1.6000E+01	2.4761E+00	1.6900E+01	2.4585E+00	1.7800E+01	2.4443E+00

As mentioned, the code is interactive allowing convenient entry of an input data file from a given set of measurements. The code is started by execution of the procedure file IUNPR2 and the correct R file designation based on cross-section library size. The code then allows a file to be built from new input.

```
-IUNPR2:P=PLOU:
 OLD OR NEW DATA SET? (O/N/EXIT)
? N
 NUMBER OF JOINTS
? 4
 EQUALLY SPACED JOINTS? (Y/N)
? N
 TYPE THE JOINTS.
? 1.2.3.9
 DEGREE OF SPLINES (1=LINEAR, ETC.)
? 2
 DO YOU WANT A TAIL? (Y/N)
? N
 DO YOU WISH THE SOLUTION TO BE PERIODIC?
? N
 DO YOU WISH TO USE TOLERANCE MULTIPLIERS? (Y/N)
? N
 MULTIPLIERS ARE ALL 1.0
 KEYWORD
? SLOPE
 INSERT, OR READ FILE? (I/R)
? I
 HOW MANY DO YOU WISH TO INSERT?
? 1
```

```
 T,FP(T),TOL=
? 2,5,5,3
 KEYWORD
? EQUALITY
 HOW MANY DO YOU WISH TO INSERT?
? 1
 T,IDERIV,VALUE=
? 2,2,5
 KEYWORD
? INEQUALITY
 HOW MANY DO YOU WISH TO INSERT?
? 1
 T,IDERIV,RELATION(+/-),VALUE=
? 5,1,+5,1
 KEYWORD
? INTEGRAL
 INTEGRAL,TOL=
? 5E10,5E9
 KEYWORD
? UNFOLD
 INSERT, OR READ FILE? (I/R)
? I
 HOW MANY DO YOU WISH TO INSERT?
? 2
 X,G(X),TOL=
? 2,5E-5,4E-6
 X,G(X),TOL=
? 5,6E-6,5E-7
 KEYWORD
? EXIT
 DO YOU WISH TO SAVE THIS DATA FILE? (Y/N)
? N
```

Typical input parameters from the REB neutron diagnostics are shown in the preceding printout. Nonsense input was entered to proceed rapidly through the input statements. There are additional input options available but these inputs typically cannot be generated from the TOF and total yield detectors.

As an example of solution data, a solution by J. M. McKenzie is presented. Here, 13 activation measurements, by Meason[18] et al from the White Sands Missile Range Fast Burst Reactor, were used to calculate the differential neutron spectrum. Specific activation was entered in units of 10^{-12} nuclides/nuclide so that the fluence values in the following printout do not have exponents. The spectral solution and the differential and integral statistics are given.

The X and G values are the cross-section file foil numbers and the specific activities, respectively. All other input and output are self-explanatory.

```
INTEGRATION:
1 2 3 4 5 6 7 8 9 10  11  12  13
EXACT CHECK=    .436E-13     PERTURBED RMS DIFF=     .273E-01

P, PRX, PRY, L, SL, S, C, POL, ALL, OR E?
? ALL
```

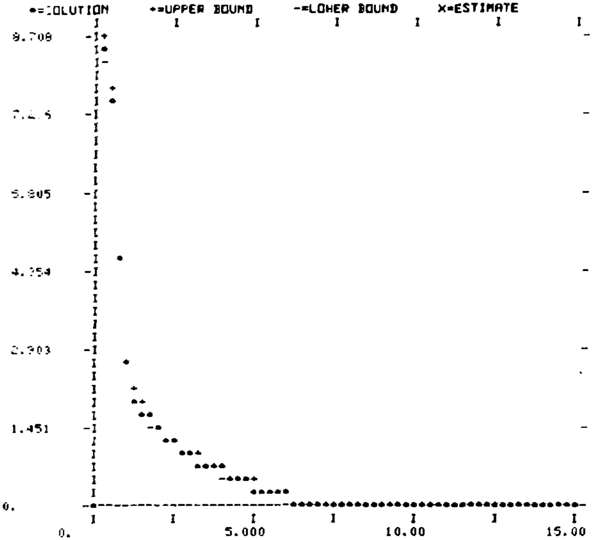


```
POINTS       ^^2^ ^                              3

SMOOTHING    ^^2^^ ^   ^        ^     ^     ^

EQUALITY     ^                    2
```

UNFOLD M= .100E+01

K	X	G	RESULT	SCALED DIF	TOL*M
1	.1000E+01	.1710E+02	.1694E+02	-.162E+00	.100E+01
2	.2000E+01	.1970E+01	.1960E+01	-.102E+00	.100E+00
3	.3000E+01	.9580E+01	.9613E+01	.657E-01	.500E+00
4	.4000E+01	.4570E+00	.4769E+00	.662E+00	.300E-01
5	.5000E+01	.1240E+02	.1253E+02	.157E+00	.800E+00
6	.6000E+01	.8160E+00	.7798E+00	-.739E+00	.490E-01
7	.7000E+01	.7960E-02	.8042E-02	.171E+00	.480E-03
8	.8000E+01	.1040E-01	.1061E-01	.350E+00	.600E-03
9	.1000E+02	.5040E-02	.4991E-02	-.164E+00	.300E-03
10	.1100E+02	.6000E+00	.5972E+00	-.768E-01	.360E-01
11	.1200E+02	.1350E+01	.1279E+01	-.706E+00	.100E+0[illegible]
12	.1300E+02	.4850E+00	.4931E+00	.407E+00	.200E-0[illegible]
13	.1400E+02	.7730E-02	.7581E-02	-.324E+00	.4[illegible]0E-0[illegible]

PROB MEAN= .8981   MEAN= -.355E-01   UNSC[illegible]LED RMS
PROB CHISQ= .9998   RMS= .393E+00   [illegible]14E 0[illegible]

SMOOTH M= .100E+01

K	T	FPP	RESULT	SCALED DIF	TOL*M
1	.5000E-01	-.1090E+04	-.1077E+04	.610E-01	.218E+03
2	.2000E+00	-.7000E+02	-.6976E+02	.175E-01	.140E+02
3	.4000E+00	-.7200E+02	-.7196E+02	.303E-02	.144E+02
4	.5500E+00	0.	-.2331E-01	-.466E-02	.500E+01
5	.7000E+00	.1800E+02	.1791E+02	-.246E-01	.350E+01
6	.9000E+00	.2100E+02	.2062E+02	-.946E-01	.400E+01
7	.1400E+01	.4600E+00	.4589E+00	-.112E-01	.100E+00
8	.2500E+01	.3000E+00	.2975E+00	-.246E-01	.100E+00
9	.5000E+01	.1400E+00	.1413E+00	.251E-01	.500E-01
10	.7000E+01	.2000E-01	.2045E-01	.447E-01	.100E-01
11	.9000E+01	.6000E-02	.5800E-02	-.100E+00	.200E-02

PROB MEAN= .9740 MEAN= -.984E-02 UNSCALED RMS
PROB CHISQ= 1.0000 RMS= .495E-01 .603E-04

INTEGRAL M= .100E+01

K		INTEGRAL	RESULT	SCALED DIF	TOL*M
1	0.	.1060E+02	.1069E+02	.158E+00	.800E+00

PROB MEAN= .8743 MEAN= .158E+00 UNSCALED RMS
PROB CHISQ= .8743 RMS= .158E+00 .949E-01